Inorganic Chemistry

Article

pubs.acs.org/IC

Synthesis and Characterization of Nonsubstituted and Substituted Proton-Conducting $La_{6-x}WO_{12-y}$

Janka Seeger,*[†] Mariya E. Ivanova,[†] Wilhelm A. Meulenberg,[†] Doris Sebold,[†] Detlev Stöver,[†] Tobias Scherb,[‡] Gerhard Schumacher,[‡] Sonia Escolástico,[§] Cecilia Solís,[§] and José M. Serra[§]

[†]Forschungszentrum Jülich GmbH, Institute of Energy and Climate Research IEK-1, D-52425 Jülich, Germany

[‡]Helmholtz-Zentrum Berlin für Materialien und Energie GmbH, Hahn-Meitner-Platz 1, D-14109 Berlin, Germany

[§]Instituto de Tecnología Química (UPV-CSIC), E-46022 Valencia, Spain

Supporting Information

ABSTRACT: Mixed proton−electron conductors (MPEC) can be used as gas separation membranes to extract hydrogen from a gas stream, for example, in a power plant. From the different MPEC, the ceramic material lanthanum tungstate presents an important mixed protonic−electronic conductivity. Lanthanum tungstate $La_{6-x}WO_{12-y}$ (with $y = 1.5x + \delta$ and $x = 0.5-0.8$) compounds were prepared with La/W ratios between 4.8 and 6.0 and sintered at temperatures between 1300 and 1500 °C in order to study the dependence of the single-phase formation region on the La/W ratio and temperature. Furthermore, compounds substituted in the La or W position were prepared. Ce, Nd, Tb, and Y were used for partial substitution at the La site, while Ir, Re, and Mo were applied for W substitution. All substituents were applied in different concentrations. The electrical conductivity of nonsubstituted $La_{6-x}WO_{12-y}$ and for all substituted $La_{6-x}WO_{12-y}$ compounds was measured in the temperature range of 400−900 °C in wet (2.5% H_2O) and dry mixtures of 4% H_2 in Ar. The greatest improvement in the electrical characteristics was found in the case of 20 mol % substitution with both Re and Mo. After treatment in 100% H_2 at 800 °C, the compounds remained unchanged as confirmed with XRD, Raman, and SEM.

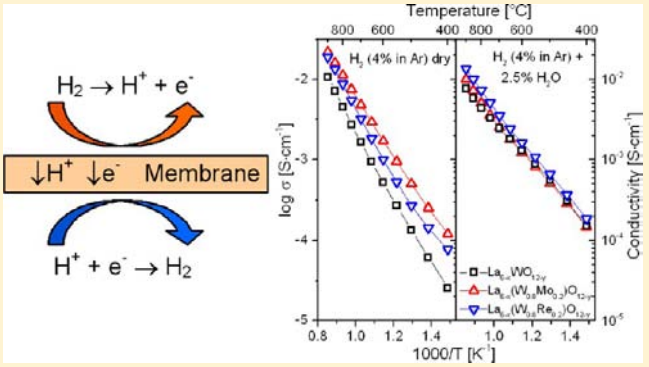

INTRODUCTION

World energy demand continues to increase and is accompanied by increased emissions of CO_2 and other greenhouse gases. One of the greatest current challenges is to improve the efficiency of energy production and hence reduce CO_2 emissions. A possible starting point to achieve this goal is use of hydrogen-based technologies. Therefore, new materials for hydrogen-related applications are needed.

Candidate materials for H_2-related applications such as proton-conducting solid oxide fuel cells (PC-SOFC),[1−3] hydrogen purification membranes,[4,5] and hydrogen separation membranes[6,7] are proton-conducting ceramics. Ceramic-based membranes offer certain benefits compared to membranes based on precious metal alloys or polymeric membranes, namely, better thermal and mechanical stability, long-term durability, as well as cost effectiveness. Depending on their chemical composition (type and valence of the dopant/substituent) and the ambient conditions (atmosphere, temperature), proton conductors exhibit pure protonic conductivity or mixed protonic−electronic conductivity. Due to their ambipolar conductivity, the mixed conductors provide net hydrogen flux through the material when a partial pressure difference is established across the membrane. Therefore, one of the most important requirements for candidates for H_2-separating membranes is that they need to have good mixed protonic−electronic conductivity, thus promoting high levels of hydrogen permeation. Furthermore, membranes for H_2 separation in power plants have to be stable in gas streams containing ash, CO, CO_2, H_2, SO_x, and high levels of moisture at elevated temperatures.

The perovskites are the most widely studied oxide-based ceramic class of materials so far. Several acceptor-doped cerates ($BaCeO_3$, $SrCeO_3$) and zirconates ($SrZrO_3$, $BaZrO_3$) show good ambipolar conductivity and relatively high hydrogen flux for this class of membrane materials.[8−16] One of the best-studied materials, the cerate $SrCe_{0.95}Tm_{0.05}O_{3-\delta}$, exhibits a hydrogen flux of 0.075 mL·min^{-1}·cm^{-2} at 900 °C and 20% H_2 in He as a feed gas, measured for a supported 0.8 mm thick membrane.[11] The material shows a total conductivity of 5×10^{-3} S·cm^{-1} at 800 °C in wet (2% H_2O) 10% H_2 in He.[17] However, the stability of cerates is a critical issue with respect to their application. They react very fast in carbon- or sulfur-containing gas streams, forming carbonates or sulfur-containing

Received: May 3, 2013
Published: September 3, 2013

 © 2013 American Chemical Society

compounds. These undesired secondary phases lead to poor conductivity and promote an overall mechanical and efficiency loss. The zirconates show appreciable stability in carbon- or sulfur-containing atmospheres and are thus suitable for application in such conditions. However, due to their high grain boundary resistances, the overall conductivity of these compounds and, furthermore, the H_2 flux is decreased. However, conductivity and hydrogen flux of the zirconates can be increased with proper substitution. One example of a cosubstituted zirconate with increased flux is $BaZr_{0.8}Y_{0.15}Mn_{0.05}O_{3-\delta}$ with a hydrogen flux of 0.011 $mL{\cdot}min^{-1}{\cdot}cm^{-2}$ for a 0.9 mm thick membrane at 900 °C and 20% H_2 in He as a feed gas. Its total conductivity in wet (2.5% H_2O) 5% H_2 at 800 °C is in the order of 10^{-2} $S{\cdot}cm^{-1}$.[16]

With respect to the drawbacks of the above-mentioned materials, the novel material class of lanthanide tungstates has been studied in recent years. A very promising material described in the literature is lanthanum tungstate with a general formula $La_{6-x}WO_{12-y}$ (with $y = 1.5x + \delta$) (termed LWO in the present paper). Its transport properties were first described by Shimura et al. in 2001.[18] They detected that the material exhibits mixed protonic−electronic conductivity with a total conductivity of 9×10^{-3} $S{\cdot}cm^{-1}$ at 900 °C in wet hydrogen. They also demonstrated that doping the material with Zr decreased the total conductivity, whereas doping with Nd does not lead to any notable effect. After this transport-oriented study, lanthanide tungstates started to attract a great deal of attention. Several research groups were simultaneously involved with the transport properties, LWO single-phase formation, as well as the structural model of this compound.

The first studies on the phase equilibriums in the La_2O_3−WO_3 system date from the 1970s.[19] Two phase diagrams were published at that time. Ivanova et al.[20] showed that there is a La_6WO_{12} phase which exists from room temperature up to 2150 °C. In contrast, Yoshimura et al.[21] showed that the $La_{10}W_2O_{21}$ phase exists up to 1740 ± 30 °C, along with the La_6WO_{12} phase formed above this temperature up to 1960 °C. More recent studies also focus on phase formation. Magrasó et al.[22] prepared the lanthanum tungstates with an atomic La/W ratio between 4.8 and 6.0 via the freeze-drying method and demonstrated that the single-phase material is only obtained when the La/W ratio is between 5.3 and 5.7 for a sintering temperature of 1500 °C. According to these authors, beyond this compositional range, segregation of either La_2O_3 (La/W ≥ 5.8) or $La_6W_2O_{15}$ (La/W ≤ 5.2) was found. Nevertheless, knowledge of the single-phase region of LWO formation depending on the sintering temperature is also very important for later production of optimized asymmetric membranes. Segregation of phases such as La_2O_3 and $La_6W_2O_{15}$ is a critical issue for membrane integrity and operation. La_2O_3 is strongly hygroscopic and when exposed to moisture forms $La(OH)_3$. Formation of this reaction product is accompanied by a volume expansion that destroys the membrane in a relatively short time. In the case of La substoichiometry, the secondary phase $La_6W_2O_{15}$ is readily formed. With increasing temperature this phase undergoes several structural transformations accompanied by extreme thermal expansion coefficient anisotropy. Therefore, its presence leads to intensive crack formation and complete disintegration of the membrane.[23]

Although it has attracted so much interest in recent years, the actual structure of the LWO compound has long remained unresolved. Finally, a solid structural model was presented by Scherb.[24] The average crystal structure of $La_{6-x}WO_{12-y}$ (with $y = 1.5x + \delta$) was described as an oxygen-deficient fluorite lattice with a doubled lattice parameter due to cation ordering. W forms a face-centered cubic (*fcc*) lattice, and the nearest W neighbors are linked by a split and half-occupied La site, which has an average oxygen coordination of seven. About one W has to be substituted by La at this site to stabilize the $La_{6-x}WO_{12-y}$ phase. The oxygen sublattice for the average crystal structure is highly disordered, especially around the W sites. These sites have 24 possible oxygen neighbors grouped around the corner of a cube with an occupancy of 25% leading to octahedral oxygen coordination for W. In Figure 1, the average crystal

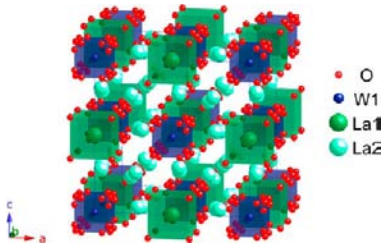

Figure 1. Model of the average crystal structure for $La_{5.4}WO_{11.1-\delta}$ in space group $Fm\bar{3}m$ with split oxygen and lanthanum sites refined from high-resolution synchrotron X-ray and neutron diffraction data according to Scherb.[24]

structure for $La_{6-x}WO_{12-y}$ is shown accordingly.[24] In parallel, Magrasó et al. carried out similar studies with three different structural models for the same $La_{6-x}WO_{12-y}$ sample. The first crystal structure was refined in space group $F\bar{4}3m$ and had W interstitials.[22] In the second model the authors corrected the former model and described the structure in a tetragonal space group and a substitution of W on La site. However, they did not publish or refine atomic coordinates.[25] Regarding the final model, which is quite similar to the model developed by Scherb, the authors describe the average crystal structure in space group $Fm\bar{3}m$ with oxygen split sites around W.[26] In comparison to the model developed by Scherb, the authors have not found La split sites, which are necessary to develop a structural model for the crystal structure on a local level.[27]

Transport properties of Ln_6WO_{12} were thoroughly studied by Haugsrud et al. in several publications.[28−30] They measured the total and protonic conductivity of undoped and 1 mol % Ca-doped Ln_6WO_{12} (stoichiometry as used in the original papers) where Ln stands for La, Nd, Gd, and Er. They found that protons dominate the conductivity over the entire low- and intermediate-temperature range up to 800 °C. At higher temperatures electronic and oxygen ionic conductivity prevails. The maximal measured protonic conductivity (σ_{H+}) was 7.5×10^{-4} $S{\cdot}cm^{-1}$ for the undoped La_6WO_{12} at 750 °C in wet (2.5% H_2O) H_2. It was furthermore shown that doping with 1 mol % Ca for Nd and 0.5 or 5 mol % Ca for La leads to a decrease in total conductivity. In contrast, doping with 1 mol % Ca for Gd and Er increased the total conductivity, although not to values higher than that of the undoped La_6WO_{12}.

In 2010, a German patent claimed the use of mixed conductive oxides based on Ln_6WO_{12},[31] reporting higher conductivities and H_2 flux levels for several substituted or doped compounds. The range of compounds covered is $(Ln_{1-x}A_x)_6(W_{1-y}B_y)_zO_{12-\delta}$ with Ln = La, Pr, Nd, Sm, A = La, Ce, Pr, Nd, Eu, Gd, Tb, Er, Yb, Ca, Mg, Sr, Ba, Th, In, Pb, B = Mo, Re, U, Cr, Nb, $0 \le x \le 0.7$, $0 \le y \le 0.5$, x or $y > 0$, $1 \le z \le 1.25$, and $0 \le \delta \le 0.3$.

dx.doi.org/10.1021/ic401104m | *Inorg. Chem.* 2013, 52, 10375−10386

Two years later, Amsif et al.[32] and Zayas-Rey et al.[33] performed substitutional experiments with LWO (termed $La_{28-y}W_{4+y}O_{54+\delta}$ and $La_{27}(W_{1-x}Nb_x)_5O_{55.55-\delta}$). Both groups used substituents already tested in the patent[31] and confirmed the increase of total conductivity by substituting the W position in LWO. Amsif et al. selected as a substituent Mo and measured the greatest improvement for a substitution amount of 40 mol %. Zayas-Rey et al. used Nb to replace W and obtained the largest increase in total conductivity for 10 and 20 mol % Nb. In contrast to substitution with Mo, where the increase in conductivity is caused by an enhancement of the electronic conductivity, substitution with Nb led to an enhancement of the oxygen ionic conductivity.

Solís et al.[34] found a clear H/D isotopic effect for the total conductivity of $La_{5.5}WO_{11.25-\delta}$ up to 750 °C, confirming the domination of proton conduction in this temperature range. Furthermore, Escolástico et al.[35−37] measured the hydrogen flux of $Nd_{5.5}WO_{11.25-\delta}$, $(Nd_{5/6}La_{1/6})_{5.5}WO_{11.25-\delta}$, and $(La_{5/6}Nd_{1/6})_{5.5}WO_{11.25-\delta}$. They detected a similar flux for the three materials, although the total conductivity of $(La_{5/6}Nd_{1/6})_{5.5}WO_{11.25-\delta}$ was clearly higher. The H_2 flux through a 0.9 mm thick $(Nd_{5/6}La_{1/6})_{5.5}WO_{11.25-\delta}$ membrane measured at 1000 °C for 50% H_2 in He in wet feed and sweep gas was 0.05 $mL\cdot min^{-1}\cdot cm^{-2}$. They also tested the stability of $Nd_{5.5}WO_{11.25-\delta}$ with respect to CO_2 and CH_4 in dry and wet environments at 700 and 800 °C and with respect to H_2S, CO_2, CO, and H_2 at 500 °C. XRD investigations after treatment showed that the material remained structurally unchanged with no indications of secondary phase formation.

As previously reported,[31] La_6WO_{12} is a relatively stable material in harsh operating conditions with promising levels of total electrical conductivity and hydrogen flux. This motivated us to carry out further work on optimizing the substitution with selected elements aiming to achieve improved electrical properties. Our research also focused on studying the temperature dependence of single LWO phase formation as well as stability in operationally relevant conditions.

EXPERIMENTAL SECTION

Sample Preparation. $La_{6-x}WO_{12-y}$ (with $y = 1.5x + \delta$, termed LWO) powder was synthesized by two different synthesis routes: the conventional solid-state reaction and the citrate-complexation route, which is a wet chemical route. Powder manufacturing via the solid-state reaction is scalable to obtain large amounts of powder. However, the major drawback of this method is the lower level of homogeneity of the product due to insufficient mixing in the solid phase. The citrate-complexation route compensates for this disadvantage: the powders produced are of a homogeneous composition, which is especially important for powders with a low concentration of substituents. However, it should be mentioned that only relatively small amounts of powder were readily producible on the lab scale in one batch.

Conventional Solid-State Route. In order to study the effect of the La/W ratio and sintering temperature on formation of single-phase LWO, powders with different La/W ratios were prepared via the solid-state reaction. Selected La/W ratios were in the range of 4.8−6.0. As starting materials La_2O_3 (Treibacher, 99.9%) and WO_3 (Fluka, 99.9%) were used. Prior use, La_2O_3 was dried at 1000 °C for 2 h. Afterward, oxides were weighed in the required stoichiometric ratios and homogenized with ethanol and milling balls. After ethanol evaporation, the starting powders were sintered at 1300, 1400, and 1500 °C for 12 h with heating and cooling rates of 2 °C/min.

Citrate-Complexation Route. The citrate-complexation route is based on the Pechini reaction.[38] The modified procedure we used was previously described by Escolástico et al.[35] The difference in our approach was addition of ethylene glycol. It was added before starting the water evaporation. After a gel had been formed, the carbon was further burned out by heating at 900 °C. Ammonium tungstate (Sigma Aldrich, 99.99%) and lanthanum nitrate (Sigma Aldrich, 99.9%) were used as precursors in this modified wet chemical synthesis. Substitutional elements were added in the form of neodymium nitrate (Alfa Aesar, 99.9%), cerium nitrate (Alfa Aesar, 99.5%), terbium nitrate (Alfa Aesar, 99.9%), yttrium oxide (Sigma Aldrich, nanopowder < 50 nm), ammonium molybdate (Sigma Aldrich, 99.9%), iridium oxide (Sigma Aldrich, 99.9%), and perrhenic acid (Alfa Aesar, 99.99%).

For the substitutional experiments, a $(La + M_{La})/W$ and $La/(W + M_W)$ ratio of 5.4 was selected, where M stands for the substituent on the La or W position. Different types of substituents were tested in three different concentrations. This starting ratio was determined by the need for a sintering temperature higher than 1400 °C in order to achieve dense samples. Powders of substituted and nonsubstituted (used as a reference composition) lanthanum tungstates were synthesized via the citrate-complexation route. Substitutions were done for both La and W but not in combination at the two sites. La was partly replaced by Nd, Ce, Tb, or Y, whereas Mo, Ir, or Re was selected for substitution at the tungsten site. The substituted amounts were 1, 5, and 17 mol % for the La site and 1, 5, and 20 mol % for the W site, respectively. For the La site, substitution with 1 mol % Al was also attempted. Since the LWO-Al powder obtained was contaminated by the secondary phase $LaAlO_3$, further experiments with Al as a substituent were not performed.

Manufacturing of Dense Ceramic Samples. In order to manufacture dense samples for further characterizations in this work, cylindrical pellets with a diameter of 28 mm and a thickness of around 3 mm were uniaxially pressed and sintered at 1500 °C for 12 h in air with heating and cooling rates of 2 °C/min. Final dimensions of samples were 16.8−17.7 mm in diameter and a thickness of around 2.7 mm. Linear shrinkage was therefore estimated to be about 37−40%. The density of the samples was determined via the Archimedes' principle using 1-propanol as a liquid media. The crystallographic density of 6.62 g/cm^3 at room temperature calculated from the crystal model by Scherb[24] was used to determine the samples relative densities. In large part the samples reached relative densities of above 97−99% of the theoretical density.

For microstructural studies, samples were prepared by embedding them in a two-component resin of Araldit DBF and hardener Aradur HY 951 and polishing them. Samples for conductivity measurements were contacted with platinum paste (Ferro GmbH) brush painted on both sides of the samples and subsequently heat treated in two steps: 1000 °C for 2 h and 1200 °C for 2 h.

Characterization Techniques. The phase composition of the manufactured powders after sintering was characterized by X-ray powder diffraction using a Bruker-AXS D4 powder diffractometer in Bragg−Brentano scattering geometry with Cu Kα (λ = 1.5418 Å) radiation. The analyzed region was between 10° and 80° 2θ with a step width of 0.02°. The resulting patterns were analyzed with Pawley fits using TOPAS software by Bruker AXS.

The microstructure of the sintered samples was investigated with a Zeiss Ulra55 SEM on embedded and polished samples. Sample porosity and pore distribution were quantified with the software "AnalySIS pro". TEM investigations were performed with a Tecnai G2 F20 (FEI) on nonsubstituted powder manufactured via the citrate-complexation route.

Thermal expansion coefficients of selected samples were measured by dilatometry with a Netzsch Dil 402 C on sintered bars with dimensions of 25 × 4 × 4 mm^3. Measurements were carried out in the temperature range from 30 to 1200 °C with a heating rate of 3 °C/min in air.

The total electrical conductivity of the synthesized materials was investigated by ac conductivity measurements at a fixed frequency of 11.9 kHz. This frequency value was selected based on preliminary measurements, which showed that it corresponds to the bulk conductivity. Conductivity was measured as a function of the temperature between 400 and 900 °C in dry and wet reducing

dx.doi.org/10.1021/ic401104m | Inorg. Chem. 2013, 52, 10375−10386

atmospheres (4% H_2 in Ar). Before supplying the gas to the sample holder, it was humidified by bubbling through water at room temperature (~2.5 vol % H_2O) or it was dried using a molecular sieve as a desiccant (ProGasMix by Norecs, Norway). Samples with coated Pt electrodes on both sides were connected to Pt nets and 4 Pt wires in pairs and finally mounted in the ProboStat holder (NorEcs, Norway). Conductivity was measured with an Alpha-A High Performance Frequency Analyzer (Novocontrol Technologies GmbH, Germany), equipped with a ZG4 test interface and controlled by WinDeta software. An oscillation voltage of 0.4 Vrms was applied, and a stray capacity of 5 pF originating from the wiring was assumed. For the measurements, the sample was heated to 900 °C at 7.5 °C/min in the required atmosphere and kept at this temperature for 11 h to reach chemical equilibrium. Conductivity was subsequently measured down to 400 °C with a step width of 50 °C.

Powder samples substituted in the W position were treated for 12 h under wet hydrogen (2.5% H_2O) at 800 °C. Samples were analyzed by XRD, SEM, and Raman spectroscopy to study the reducibility and stability of the samples. Raman analysis was performed with a Renishaw inVia Raman spectrometer equipped with a Leica DMLM microscope and a 514 nm Ar^+ ion laser as an excitation source. A 50× objective of 8 mm optical length was used to focus the depolarized laser beam on a spot 3 μm in diameter. A CCD array detector was used for Raman scattering collection.

RESULTS AND DISCUSSION

Structural Characterization (XRD). With the aim of studying the effect of the La/W ratio on the LWO single-phase formation region in depth, the manufactured nonsubstituted LWO powders with La/W ratios of 4.8−6.0 were investigated via XRD. In the present work, the compositions were named LWO*z*, where *z* corresponds to the La/W ratio. The average crystal structure of LWO is an oxygen-deficient cubic fluorite lattice. However, detailed structural investigations of single-phase LWO will be discussed elsewhere.[27]

XRD patterns were collected for phase identification. XRD patterns for LWO6.0 (a), LWO5.4 (b), and LWO4.8 (c) sintered at 1500 °C are shown in Figure 2. Depending on the

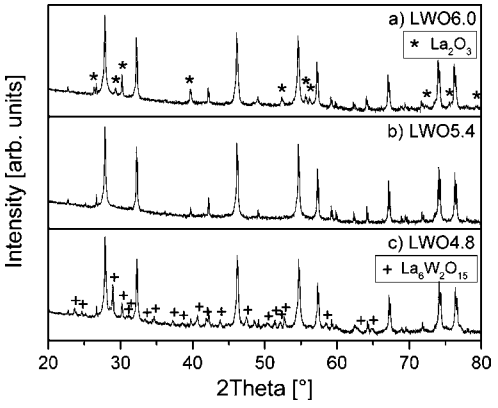

Figure 2. XRD pattern presented in log scale of samples with different La/W ratios sintered at 1500 °C for 12 h: La/W = 6.0, $La_{6-x}WO_{12-y}$ + La_2O_3 (a), La/W = 5.4, single-phase $La_{6-x}WO_{12-y}$ (b), and La/W = 4.8, $La_{6-x}WO_{12-y}$ + $La_6W_2O_{15}$ (c).

La/W ratio, different phases can be distinguished: LWO + La_2O_3 for La/W = 6.0 (a), single-phase LWO for La/W = 5.4 (b), and LWO + $La_6W_2O_{15}$ for La/W = 4.8 (c). Figure 3 shows the region of single-phase LWO for different sintering temperatures as a function of the corresponding La/W ratio. It can be seen that the single-phase region depends not only on the La/W ratio but also on the sintering temperature. With

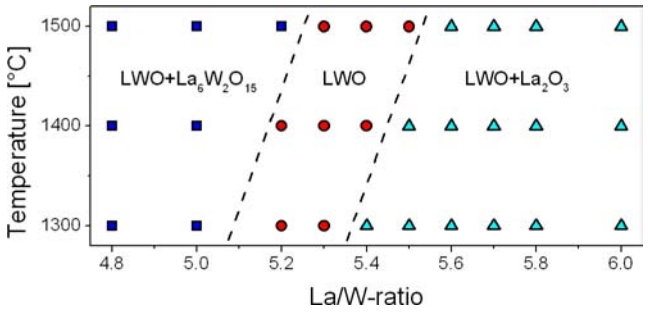

Figure 3. Single-phase region of LWO powders plotted against the La/W ratio and sintering temperature (heating and cooling rate 2 °C/min).

increasing sintering temperature the single-phase region shifts to higher amounts of lanthanum. At 1300 °C it lies between 5.2 and 5.3, whereas at 1500 °C it is between 5.3 and 5.5. This shift could be ascribed to the metastability of some LWO compositions and explained by a combination of two coupled effects: (i) the small grain size, which stabilizes some crystal structures (by analogy with ZrO_2); (ii) the most likely incomplete interdiffusion of La and W cations, which does not achieve the final equilibrium position as described in recent structural studies.[24,25] Magrasó et al.[22] performed similar experiments with powder produced via the freeze-drying method and sintered at 1500 °C. They showed a single-phase region at that temperature between La/W = 5.3 and La/W = 5.7. In contrast, we observed that the single-phase region is narrower. In our study, the LWO5.6 and LWO5.7 samples showed traces of La_2O_3 identified in the XRD pattern.

After sintering at 1500 °C, the substituted powder samples were also studied by XRD. Certain compositions were resynthesized with modified La/W ratios because the single-phase region shifted upon substitution. Powders obtained with the selected La/W ratios, corresponding powder names, and crystal phases formed are shown in Table 1. Most of the powders were single phase, and they were used for further investigations in microstructural and conductivity studies. Corresponding indications are given in the table.

Partial substitution of La or W in LWO is expected to promote changes in the lattice parameter of the unit cell due to the different ionic radii of the substituted and substituting ions. These changes can have a direct influence on the transport properties of the materials, as observed in other materials.[35,39] The ionic radii of La, W, and various substituents are summarized in Table 2 by taking into account the 6- or 7-fold coordination of the ions.[40] Figure 4 summarizes the cell parameter changes for the different $(La_{1-z}M_z)_{6-x}WO_{12-y}$ substituted compounds. The cell parameter decreases linearly when the substitution amount increases as a consequence of the smaller ionic radii of the substituents (Ce, Nd, Tb, and Y) compared to that of La (Figure 4a). By comparing the cell parameters of the 17 mol % substituted compounds as a function of ionic radii (for +3 and +4 oxidation states, Figure 4c), a linear relationship can be found between the ionic radii in the +3 state and the cell parameters. This indicates that in LWO-Tb17 most Tb is in the +3 oxidation state. (Note that in the graph of Figure 4c Tb is the only ion that can be in both oxidation states.) Figure 4b shows a similar analysis for 1 mol % substitution. A linear relationship of the cell parameters with the ionic radii can also be found by taking into account the fact that Ce and Tb are in mixtures of +3 and +4 oxidation states.

dx.doi.org/10.1021/ic401104m | Inorg. Chem. 2013, 52, 10375−10386

Table 1. Summary of Data About $(La + M_{La})/W$ or $La/(W + M_W)$ Ratios, Crystal Phases Obtained after Sintering at 1500 °C for 12 h, and Use for Further Investigations of Substituted $(La_{1-z}M_z)_{6-x}WO_{12-y}$ and $La_{6-x}W_{1-z}M_zO_{12-y}$ Powders Produced via the Citrate-Complexation Route

		1 mol %				5 mol %				17 mol %			
	substituent	$La + M_{La}/W$	crystal phases	use	sample name	$La + M_{La}/W$	crystal phases	use	sample name	$La + M_{La}/W$	crystal phases	use	sample name
La	Nd	5.4	LWO	yes	LWO-Nd1	5.4	LWO	yes	LWO-Nd5	5.4	LWO	yes	LWO-Nd17
	Ce	5.4	LWO	yes	LWO-Ce1	5.8[a]	LWO	yes	LWO-Ce5	5.4–6.0[a]	LWO + $La_6W_2O_{15}$	no	
	Tb	5.4	LWO	yes	LWO-Tb1	5.4	LWO	yes	LWO-Tb5	5.4	LWO	yes	LWO-Tb17
	Y	5.4	LWO	yes	LWO-Y1	5.4	LWO	yes	LWO-Y5	5.4	LWO	yes	LWO-Y17
		1 mol %				5 mol %				20 mol %			
	substituent	$La/W + M_W$	crystal phases	use	sample name	$La/W + M_W$	crystal phases	use	sample name	$La/W + M_W$	crystal phases	use	sample name
W	Mo	5.4	LWO	yes	LWO-Mo1	5.4	LWO	yes	LWO-Mo5	5.4	LWO	yes	LWO-Mo20
	Ir	5.4	LWO	yes	LWO-Ir1	5.2[a]	LWO	yes	LWO-Ir5	5.4–5.2[a]	LWO + La_2O_3	no	
	Re	5.4	LWO	yes	LWO-Re1	5.4	LWO	yes	LWO-Re5	5.2[a]	LWO + $La_6W_2O_{15}$	yes	LWO-Re20

[a]Resynthesis of the composition with modified La/W ratios because of shifted single-phase region.

Table 2. Shannon Ionic Radii[40] of the Different Ions for 7-Fold Coordination (when substituting La) and 6-Fold Coordination (when substituting W)

Shannon ionic radius for 7-fold coordination [Å]					
electron charge	La	Ce	Nd	Tb	Y
3	1.100	1.070	1.045[a]	0.980	0.96
4		0.920[a]		0.820[a]	
Shannon ionic radius for 6-fold coordination [Å]					
electron charge	W	Mo	Ir	Re	
4	0.660	0.650	0.68	0.630	
5	0.620	0.610	0.625	0.580	
6	0.600	0.590	0.570	0.550	

[a]Interpolated.

This indicates that the +3 oxidation state prevails when the amount of substituted ions is higher as a direct consequent of the stability of the structure.

Microstructural Study. Powders produced via the citrate-complexation route were studied by TEM as can be seen in Figure 5 for the nonsubstituted LWO5.4. The powders present a mean particle size of around 50 nm after thermal treatment at 900 °C. Usually, the average grain size of the powders produced by the two routes differs greatly. However, direct comparison is not possible in this case due to the specifics of the powder preparation (powders produced via the citrate-complexation route were calcined at 900 °C, while the solid-state reaction powders were treated at 1300–1400 °C at least). Furthermore, samples produced via the solid-state reaction were only used in the phase formation study, while samples made via the citrate-complexation route were used in the electrical study. Therefore, the microstructural study performed on samples produced by the citrate-complexation route is more relevant to the properties of the studied materials.

The microstructure of substituted and nonsubstituted samples prepared via the citrate-complexation route, sintered at 1500 °C for 12 h, and subsequently polished were studied by SEM. Figure 6 shows images with improved crystal-orientation contrast. Images with original and improved contrast are also presented in the Supporting Information, Figures S1 and S2. As can be seen from Figure 6a, nonsubstituted LWO5.4 exhibits a dense microstructure with a mean grain size in the range from 6 to 12 μm. The grains predominantly take the form of irregular hexagons to minimize the grain-boundary free energy of the single grains. Pores are located within the grain interior, while no pores were observed at the grain boundaries. However, the

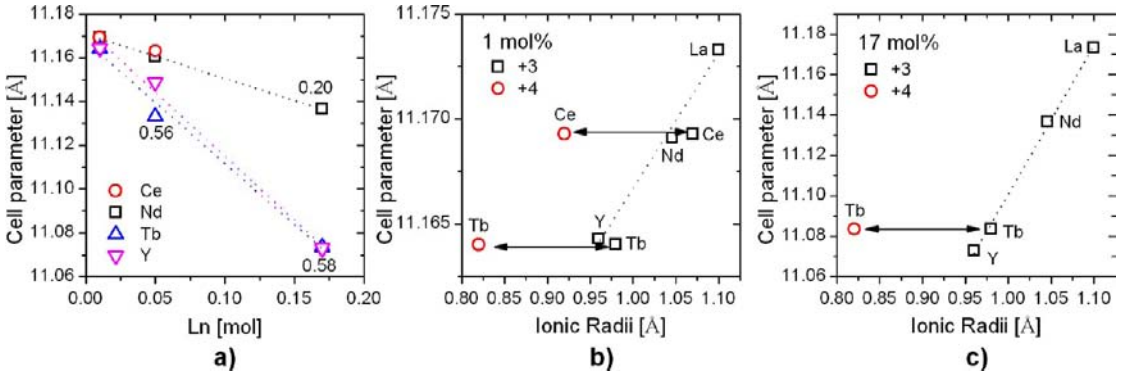

Figure 4. Evolution of the cell parameter determined by XRD for samples substituted at the La site as a function of the amount of substituent (a) and ionic charge and ionic radius of the substituents for 1 (b) and 17 mol % (c) substituted compositions; dotted lines and numbers represent Vegard's slopes (a).

dx.doi.org/10.1021/ic401104m | Inorg. Chem. 2013, 52, 10375–10386

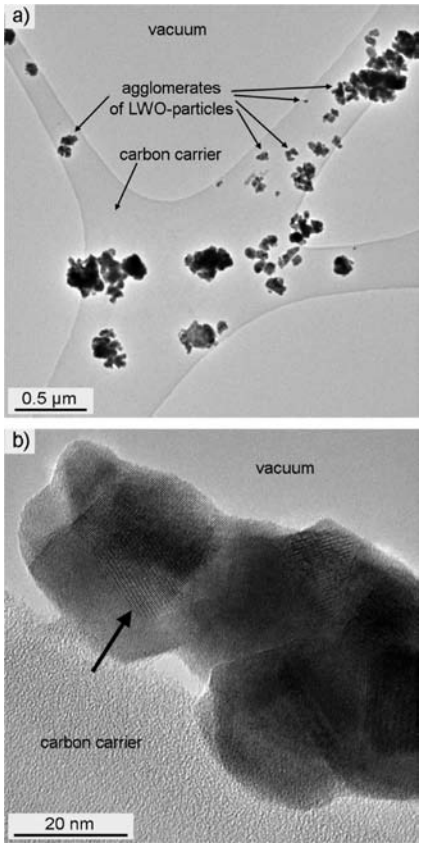

Figure 5. TEM images at different magnifications of LWO5.4 powder produced via the citrate-complexation route and calcined at 900 °C. Lattice planes are visible (marked by an arrow) (b).

pores are small with a mean pore size below 1 μm, and the porosity of the material was estimated to be below 1%.

The microstructure of selected examples of substituted LWO compounds (Ce-, Nd-, Mo-, and Re-substituted LWO) is shown in Figure 6b–e. The SEM study reveals similar microstructural characteristics such as high density (above 97%), small pores within the grain interior rather than at the grain boundaries, as well as hexagonal grain shape and mean grain size of the same magnitude as observed for the nonsubstituted material. The porosity of LWO-Ce1 is estimated to be slightly higher (1.5%).

Sample LWO-Re20 was additionally studied by EDX. Results are presented in the Supporting Information, Figure S3. The presence of $La_6W_2O_{15}$ was confirmed, which was in agreement with the XRD results that indicated traces of this secondary phase. The dark phase on the micrographs was identified as the main LWO phase, while the phase in light gray was defined as the secondary $La_6W_2O_{15}$ phase. The grain size of the darker phase of LWO-Re20 (Figure 6e) is smaller compared to the single-phase samples and was detected between 6 and 9 μm. The average size of the light gray grains composed of the secondary phase is even smaller at around 2 μm.

Furthermore, it was found that the secondary phase is characterized by La depletion and enrichment of W and Re. Accumulation of Re was disproportionally higher than accumulation of W. There are two possible explanations for this behavior. First, the solubility limit of Re in LWO could have been exceeded. Then the excessive Re is accumulated in the secondary phase. Second, the difference in the crystal structures of LWO and $La_6W_2O_{15}$ could offer an explanation. LWO has a close-packed cubic structure, whereas the structure of $La_6W_2O_{15}$ contains ordered [La–O] units that form $(La_3O_2)_\infty$ double chains and disordered $[WO_{5.5}]$ tetrahedrons. Rhenium itself readily forms inorganic polymers (for example, as Re_2O_7) and could therefore be more easily incorporated within the relatively open $La_6W_2O_{15}$ structure than within the LWO lattice, thus favoring generation of $La_6W_2O_{15}$ as a secondary phase.

Thermal Expansion Coefficient. The thermal expansion coefficients (TEC) of LWO5.4, LWO-Mo20, and LWO-Re20, measured from 30 to 1200 °C are between 10.1×10^{-6} and 11.7×10^{-6} K^{-1} over the whole measured temperature range as shown in Figure 7. These values are very similar to the relative expansion of the cell parameter obtained for LWO5.5 based on HT-XRD, which has a value of 11.1×10^{-6} K^{-1} regardless of the studied atmospheres.[41] Furthermore, the TEC increases with temperature, and this fact may be attributed to loss of lattice oxygen and formation of oxygen vacancies at high temperatures. On the other hand, Re- and Mo-substituted compounds have a slightly lower TEC than the nonsubstituted compound, and this fact can be ascribed to the lower ionic radii of Re and Mo in comparison to the substituted W. Thermal expansion coefficients of compounds studied here and other conventional ceramic materials are listed in Table 3. Barium zirconate has the smallest thermal expansion of all the compared materials with $\alpha = 7.1 \times 10^{-6}$ K^{-1}. By doping the material with Y the thermal expansion coefficient increases. Thermal expansion of LWO lies in the same region as 8YSZ and barium cerate and is smaller than the corresponding regions of MgO and a composite of NiO and 8YSZ.

Electrical Conductivity Study. The total conductivities of nonsubstituted LWO5.4 and all substituted LWOs summarized in Table 1 were measured as a function of temperature in dry and wet Ar/H_2.

Substitution at Lanthanum (La) Position. Figure 8 shows the total conductivities for 1 mol % La-site-substituted LWO compounds in dry and wet Ar/H_2 plotted as a function of the inverse temperature. Partial substitution of La by the selected ions does not bring about any improvement to the total conductivity of LWO as can be observed from the figure. In fact, the conductivity for all compounds is lower in both atmospheres than that measured for LWO5.4 (black squares in the graph). Furthermore, no improvement of the conductivity is achieved by increasing the amount of substituent (5 and 17 mol %). This effect can be related to the lower ionic radii of the substituting cations in comparison with La, which causes the lower cell parameter as can be observed in Figure 4.[37]

A comparison between the total conductivities in wet and dry Ar/H_2 for the nonsubstituted LWO5.4 (Figure 9a) and additionally for all 1 mol % La-substituted LWOs (Figure 9b–e) is presented in Figure 9.

Results obtained for the nonsubstituted LWO5.4 are very similar to those reported previously for LWO5.5.[34] Below 700–800 °C, depending on the specific material composition, the total conductivity in wet atmosphere is higher compared to that in dry atmosphere. This fact can be ascribed to the protonic conductivity as a result of sample hydration in the presence of hydrogen and water according to the well-known equations

$$H_2O(g) + v_O^{\bullet\bullet} + O_O^x \Leftrightarrow 2OH_O^{\bullet} \quad (1)$$

$$H_2 + 2O_O^x \Leftrightarrow 2OH_O^{\bullet} + 2e^{/} \quad (2)$$

dx.doi.org/10.1021/ic401104m | Inorg. Chem. 2013, 52, 10375–10386

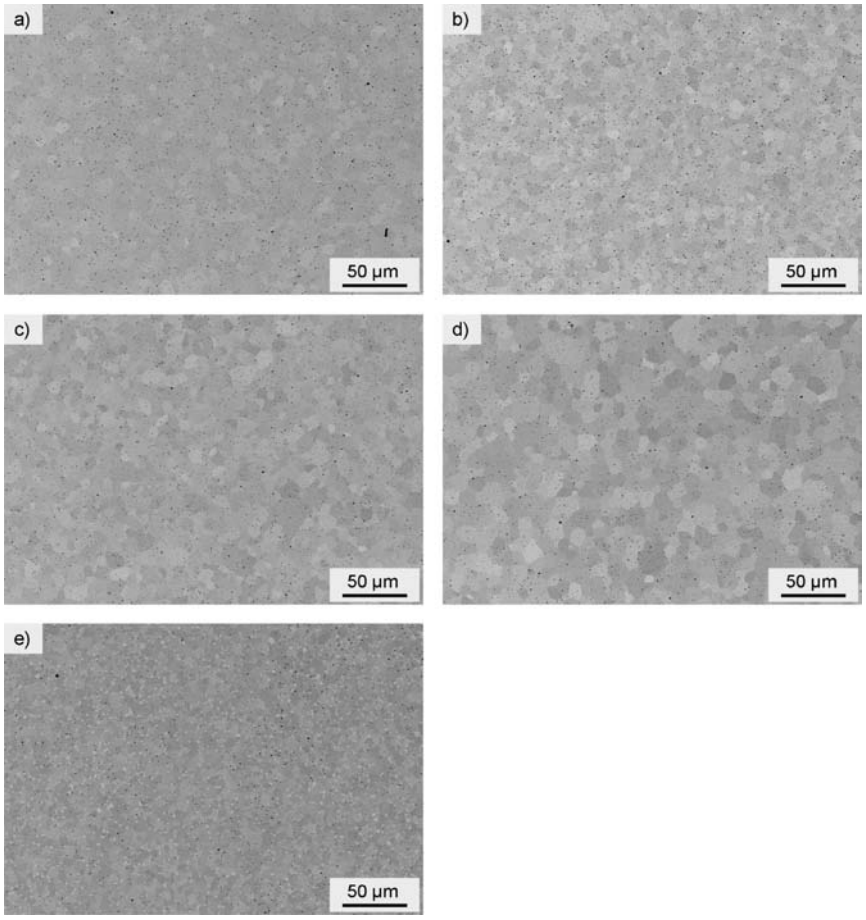

Figure 6. SEM images of polished cross sections of LWO5.4 (a), LWO-Ce1 (b), LWO-Nd1 (c), LWO-Mo20 (d), and LWO-Re20 (e) sintered at 1500 °C for 12 h with improved crystal-orientation contrast.

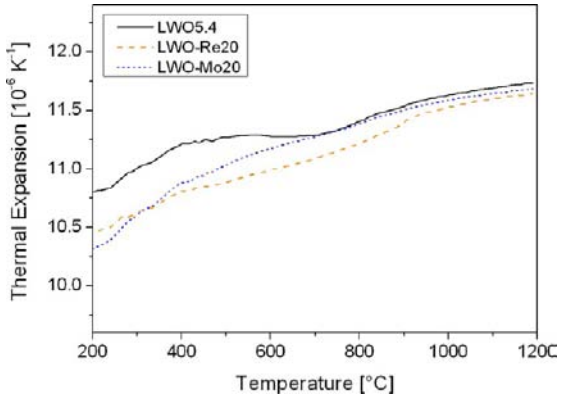

Figure 7. Thermal expansion as a function of temperature determined for nonsubstituted LWO5.4 sample and Re- and Mo-substituted LWOs.

At temperatures higher than 700−800 °C (depending on the substituting cation), the conductivity becomes independent of $p(H_2O)$: similar values are observed in dry and wet conditions. This effect is ascribed to the drop in proton concentration with increasing temperature due to the exothermic nature of hydration. At elevated temperatures the conductivity of the protons is no longer the dominating term but oxygen ionic and n-type electronic partial conductivities come into play according to the equation

Table 3. Linear Thermal Expansion Coefficients (TEC) of Conventional Ceramic Materials from the Literature and Materials Developed in the Present Work

material	TEC α [K^{-1}]	remperature region	ref
$BaZrO_3$	7.1×10^{-6}	25−727 °C	42
$BaZr_{0.85}Y_{0.15}O_{3-\delta}$	9×10^{-6}	30−1000 °C	43
8YSZ	10.9×10^{-6}	30−1000 °C	44
$BaCeO_3$	11.2×10^{-6}	25−727 °C	42
NiO-8YSZ-substrate	12.6×10^{-6}	30−1000 °C	44
MgO	13.9×10^{-6}	25−1000 °C	8 in 45
LWO-Re20	11.6×10^{-6}	30−1200 °C	this work
LWO-Mo20	11.7×10^{-6}	30−1200 °C	this work
LWO5.4	11.7×10^{-6}	30−1200 °C	this work

$$O_O^x \Leftrightarrow v_O^{\bullet\bullet} + 2e' + \frac{1}{2}O_2(g) \quad (3)$$

The electrical behavior of all 1 mol % substituted LWO compounds is very similar to that observed for the nonsubstituted LWO, i.e., at lower temperatures the proton conductivity prevails, whereas at high temperatures the materials become predominantly oxygen ionic and n-type electronic conductors (eqs 1−3). The conductivities in wet atmosphere measured in the intermediate-temperature (IT) range (400−600 °C) follow the sequence Y-, Tb-, Nd-, and Ce-substituted LWO and lie between 10^{-4} and 10^{-3} $S \cdot cm^{-1}$. All substituted compounds present an important proton contribution in the IT range, as can be inferred from the magnitude of

dx.doi.org/10.1021/ic401104m | Inorg. Chem. 2013, 52, 10375−10386

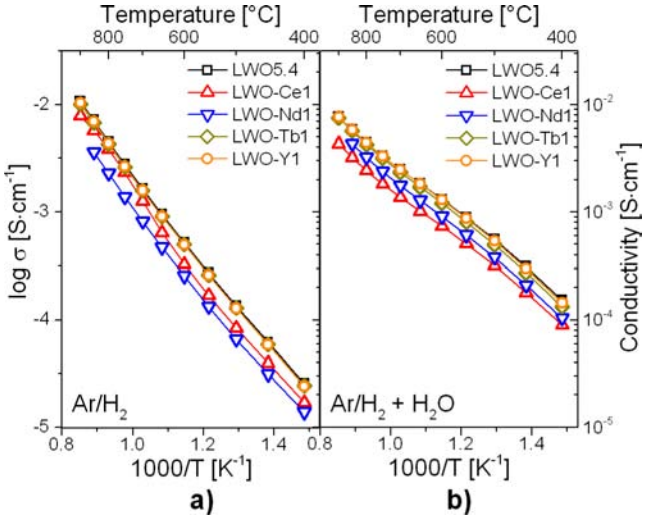

Figure 8. Temperature dependence of the total conductivity of LWO, 1 mol % substituted on the La site in dry (a) and wet (b) Ar/H_2 compared with nonsubstituted LWO5.4.

the hydration effect, which is very similar to that corresponding to the nonsubstituted LWO. In the case of Y as substituent, the hydration effect is slightly higher than in the rest of the compounds.

By substituting the selected elements at the La position it was expected that this would affect both the local structure and the electrical balance by generating defects. The ionic radius of La^{3+}-site substituents decreases in the order Ce^{3+}, $Ce^{4+} \rightarrow Nd^{3+} \rightarrow Tb^{3+}$, $Tb^{4+} \rightarrow Y^{3+}$, as already seen in Table 3. The observed total conductivity in the IT range in wet atmosphere follows the opposite tendency, i.e., increases with decreasing ionic radius. It could be therefore speculated that when La-site substitution is envisaged, the smaller ionic radius of the substituent may be beneficial due to generation of loosely packed local arrangements.

Another trend is the observed effect of the substituent type on the transport mechanism. The highest conductivity in dependence of the atmosphere reflects the dominating charge carriers. As it can be seen from the graph (Figure 9), the temperature at which the conductivity in dry conditions becomes higher than that in wet atmosphere changes with the type of substitution. This transition temperature is around 800 °C for all compounds except for LWO-Ce1, where the change ($\sigma_{Ar/H_2} > \sigma_{Ar/H_2+H_2O}$) occurs at around 700 °C. This lower temperature can be due to the Ce reducibility, which produces an increase of the electronic and/or oxygen ion conductivity. At higher temperatures (above 600−700 °C), the conductivity in dry Ar/H_2 is clearly increased compared to that in wet Ar/H_2, hence showing an increased n-type electronic conductivity at elevated temperatures. Furthermore, the associated activation energy for conductivity (Figure 8) does not show any dependence upon the substitutional type, except for a very slight dependence for Ce in dry atmosphere.

Substitution at Tungsten (W) Position. LWO was partially substituted in the W position using Ir, Re, and Mo. Selected concentrations were 1 and 5 mol % for Ir and 1, 5, and 20 mol % for Re and Mo.

Figure 10 presents the total conductivity of the Ir-substituted LWOs as a function of temperature measured in dry Ar/H_2 (a) and wet Ar/H_2 (b) compared with the nonsubstituted LWO (in black). Figure 10c presents a summary of all tested Ir-substituted compounds. The similar Figures 11 and 12 depict conductivities for Re- and Mo-substituted LWOs.

As can be observed in Figure 10, Ir substitution did not lead to any appreciable changes in LWO total conductivity. At temperatures higher than ~650 °C in a wet atmosphere, there is a slight increase in the conductivity of the 1 mol % substituted compound (Figure 10b) compared to the nonsubstituted LWO (Figure 9a), most probably attributable to the higher electronic conductivity resulting from Ir substitution. However, the overall conductivity decreases with increasing substituent concentration. This effect is more obvious in a wet atmosphere as shown in Figure 10b. The temperature at which

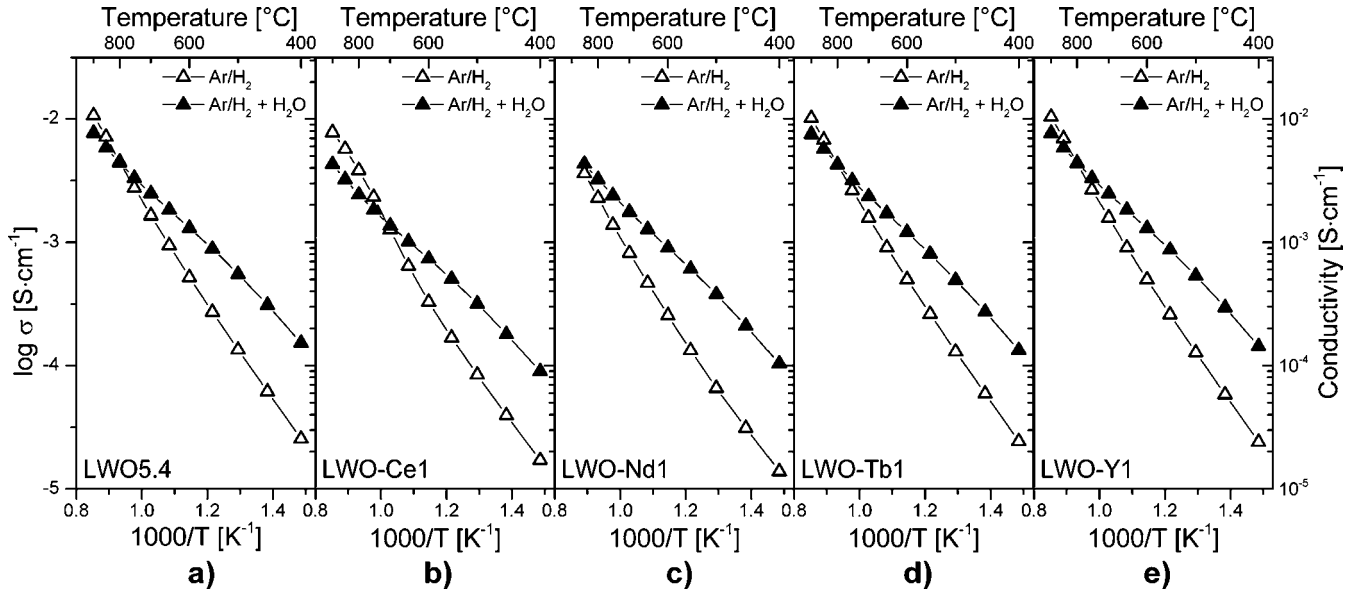

Figure 9. Total conductivity of LWO, 1 mol % substituted on the La site in dry and wet Ar/H_2 as a function of the inverse temperature; nonsubstituted LWO5.4 (a), replaced by 1 mol % Ce (b), Nd (c), Tb (d), and Y (e).

dx.doi.org/10.1021/ic401104m | *Inorg. Chem.* 2013, 52, 10375−10386

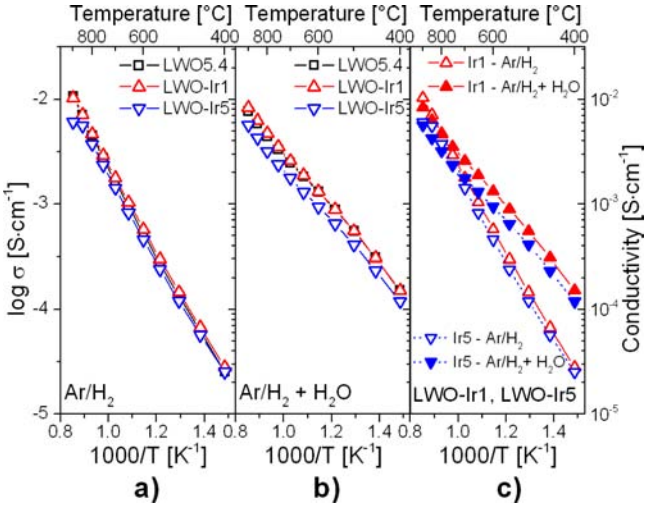

Figure 10. Temperature dependence of the total conductivity of Ir-substituted LWO in dry Ar/H_2 (a) and wet Ar/H_2 (b) compared with nonsubstituted LWO5.4; comparison between the two atmospheres (c).

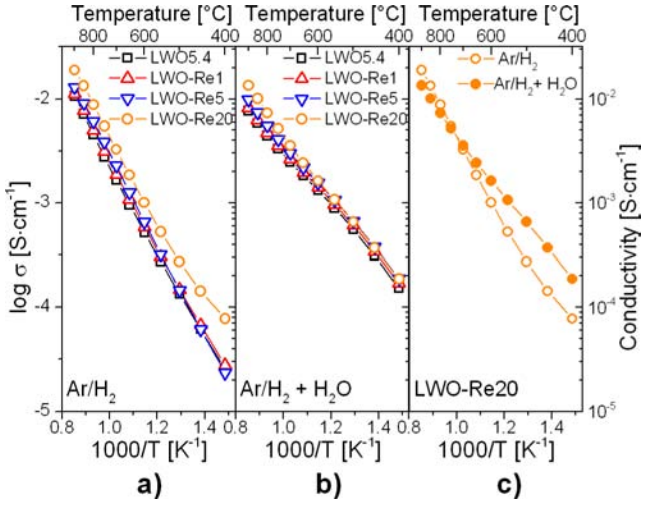

Figure 11. Temperature dependence of the total conductivity of Re-substituted LWO in dry Ar/H_2 (a) and wet Ar/H_2 (b) compared with nonsubstituted LWO5.4; comparison between the two atmospheres for 20 mol % Re-substituted LWO (c).

the transport mechanism changes, as already discussed in the previous section, is in this case about 800 °C. This value is relatively high, corresponding to a higher thermodynamic stability of the generated proton defects. The hydration effect decreases slightly with an increase of the substituent concentration from 1 to 5 mol % as can be seen from Figure 10c.

Substitution with Re at the W site led to an improvement of the LWO conductivity for the two experimental atmospheres (Figure 11). Improvement was also observed for the three tested compounds with different Re concentrations. In dry atmosphere the most effective was the case with 20 mol % Re substituent (Figure 11a). Under wet environments and in the IT range, LWO-Re5 and LWO-Re20 showed similar effects (Figure 11b). At temperatures above 550−600 °C, the higher Re concentration marks a more appreciable effect. The increase of conductivity as a function of substituent concentration is stronger in dry conditions and can be related to the

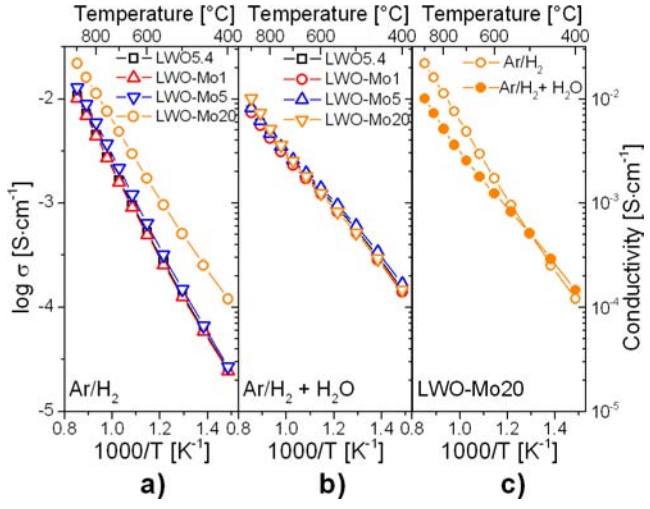

Figure 12. Temperature dependence of the total conductivity of Mo-substituted LWO in dry Ar/H_2 (a) and wet Ar/H_2 (b) compared with nonsubstituted LWO5.4; comparison between the two atmospheres for 20 mol % Mo-substituted LWO (c).

enhancement of the n-type electronic conductivity ascribed to the Re reducibility. This hypothesis is in agreement with the lower hydration effect observed for LWO-Re20 (Figure 11c and Supporting Information, Figure S4) compared to the non-substituted compound shown in Figure 9a. Furthermore, the temperature at which conductivity in dry atmosphere exceeds that in wet atmosphere is around 700 °C, and it is lower for LWO-Re20 than for LWO5.4 at around 800 °C.

In the case of Mo substitution, an improvement of the conductivity was also observed in both atmospheres and the effect was expressed more clearly in dry Ar/H_2 (Figure 12a and 12b). As discussed for Re, the increase in total conductivity can be ascribed to promotion of n-type electronic conductivity due to Mo reducibility. The magnitude of the hydration effect is very similar for LWO-Mo1 and LWO-Mo5, whereas for the compound with 20 mol % Mo the conductivity in dry conditions already exceeds that in wet conditions at around 500 °C as can be observed in Figure 12c (and in the Supporting Information, Figure S5). This behavior indicates predominantly oxygen ionic and/or n-type electronic conductivity in the case of Mo-substituted LWO, which displays an increase with increasing concentration of the substituent from 1 to 5 mol %. It may be concluded that this is the opposite tendency to that observed in the case of Ir-substituted LWO. Finally, samples with 20 mol % Re and 20 mol % Mo exhibit relatively similar behavior.

Stability. In order to study the reducibility of the LWO-based samples with substitution of the W position and also to support the hypothesis about the increase of electronic and oxygen ionic conductivity, samples were treated for 12 h in wet hydrogen at 800 °C. XRD and Raman spectroscopy studies and SEM investigations were performed.

XRD patterns of substituted samples before and after treatment are plotted in Figure 13. For Re-substituted compounds, peaks shift to lower diffraction angles when the materials are treated in wet hydrogen (Figure 13a). The observed shift can be directly ascribed to Re reduction ($Re^{6+} \rightarrow Re^{5+} \rightarrow Re^{4+}$) due to the higher ionic radii of the reduced cations (Re^{5+}, Re^{4+}) with the consequent increase of the cell parameter. An appreciable hydration of the sample is not

dx.doi.org/10.1021/ic401104m | Inorg. Chem. 2013, 52, 10375−10386

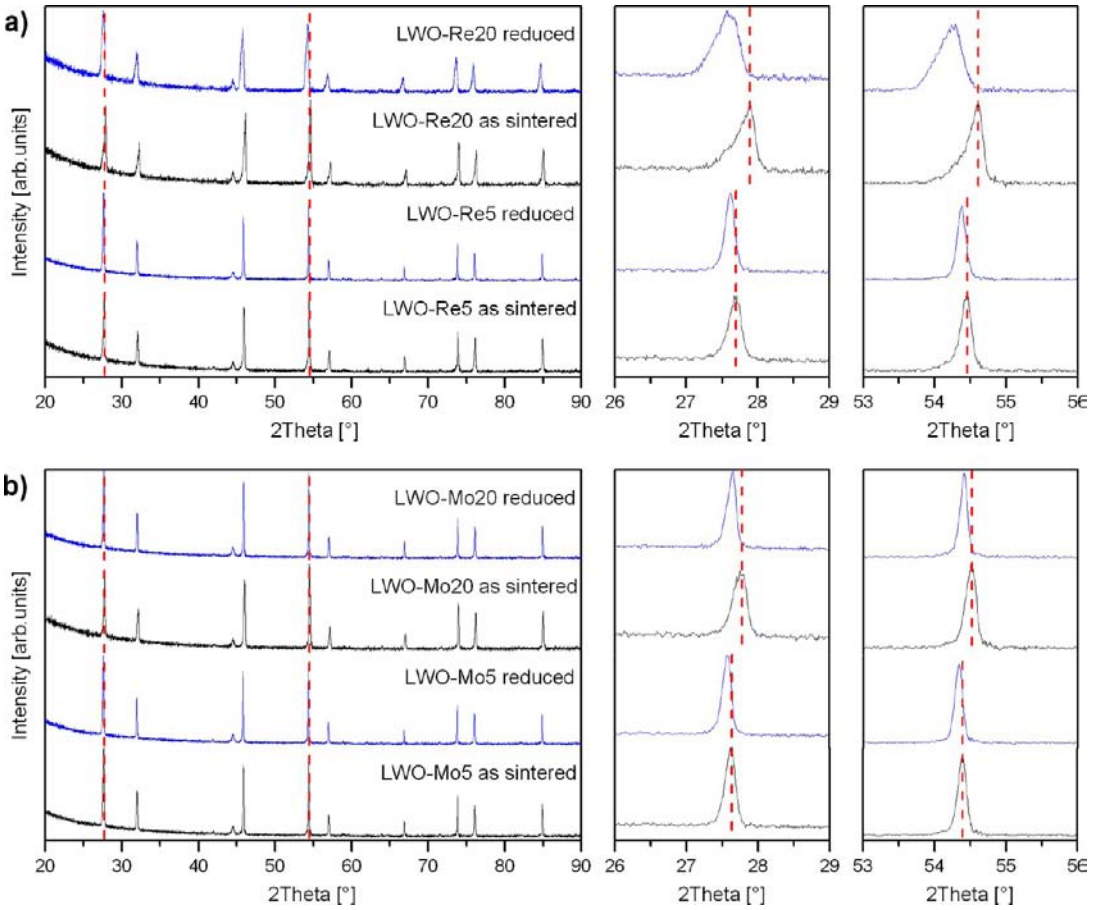

Figure 13. XRD patterns of Re- (a) and Mo-substituted (b) LWO compounds before and after reducing treatment in 100% H_2 at 800 °C for 12 h.

expected due to the high temperature of the treatment that prevents incorporation of water. The magnitude of the observed shift was higher in LWO-Re20 than in LWO-Re5. This can be explained by the higher amount of reduced Re. The same behavior can be observed for the Mo-substituted compound (Figure 13b), where a slight shift of the diffraction peaks to the left (toward the higher cell parameter) is observed after the reducing treatment.

The diffraction peaks for LWO-Re20 are broader than those obtained for LWO-Re5 compound. This fact could be assigned to the evolution of the symmetry from cubic to rhombohedral upon increasing Re concentration. In fact, compounds with general formula $Ln_{6-x}ReO_{12-y}$, where Ln = Ho, Er, Tm, Yb, and Lu, have rhombohedral symmetry as reported by Hartmann et al.[46]

Figure 14 presents results of Raman experiments carried out on Re- and Mo-substituted LWO, respectively, before and after reduction. As it can be seen from the figure, slight shifts to smaller wavelengths can be detected in the Raman peak registered at 800 cm^{-1} after the samples were exposed to reducing conditions. This peak at 800 cm^{-1} corresponds to the stretching mode ν(O−W−O),[47] and the observed peak shift is ascribed to the increase in the cell parameter produced by Re and Mo reduction, respectively. From this experiment, it can also be ascertained that during the reducing treatments formation of secondary phases does not occur and exclusively the original structural peaks appear in the Raman spectra. Reduction of Re and Mo cations, when they are used as

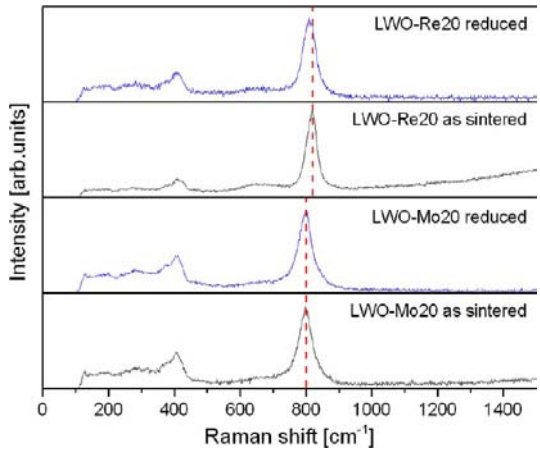

Figure 14. Raman spectroscopy of Re- and Mo-substituted LWO compounds before and after reducing treatment in 100% H_2 at 800 °C for 12 h.

substituents in LWO, was also observed by TPR analysis in a previous study.[48]

Comparison of the SEM images of the substituted powders show no differences before and after treatment in wet hydrogen (Figure 15 and Supporting Information, Figures S6 and S7). It can be observed that there are no metal dispersions after reduction. Moreover, the distinguishable lines in the images can already be found before reduction and also for both substitutional elements. This means that they are due to neither any metal incorporation nor the reduction of metal.

dx.doi.org/10.1021/ic401104m | Inorg. Chem. 2013, 52, 10375−10386

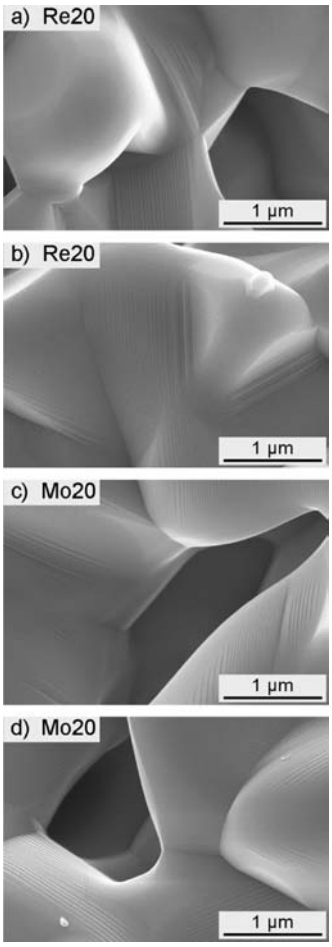

Figure 15. SEM images of the powder surfaces before (a, c) and after (b, d) reducing treatment in 100% H_2 at 800 °C for 12 h: LWO-Re20 (a, b), LWO-Mo20 (c, d). Powders were produced via the citrate-complexation route.

CONCLUSIONS AND OUTLOOK

In the present work, nonsubstituted and substituted LWO-based proton conductors were synthetized. Their phase compositions and microstructural and electrical properties were thoroughly studied and discussed. XRD analysis of a series of nonsubstituted LWO compounds revealed that single-phase material was formed within a specific La/W ratio range and that this is significantly lower than 6. Moreover, the range of La/W ratios yielding a stable single-phase structure depends on the sintering temperature, and the range shifts to a higher ratio with increasing sintering temperatures. Specifically, at 1300 °C a single-phase material was synthesized with La/W = 5.2−5.3, whereas at 1500 °C the La/W ratio was between 5.3 and 5.5. Since a sintering temperature of at least 1400 °C is needed to manufacture dense samples, a La/W ratio of 5.4 is recommended.

Compounds with partial substitution of the La site by Ce, Nd, Tb, or Y and of the W site by Ir, Mo, or Re were produced with different concentrations of the substituent. All substituted samples have single-phase composition and exhibit dense microstructure with a porosity of less than 2%, as confirmed by XRD and SEM analyses. The exception is the 20 mol % Re-substituted LWO sample, which shows traces of the secondary $La_6W_2O_{15}$ phase. The electrical behavior of all substituted samples was studied by means of ac conductivity tests carried out in wet (2.5% H_2O) and dry H_2 (4% in Ar) from 400 to 900 °C. Conductivity results were compared to the nonsubstituted LWO5.4, which was selected as a reference compound. No increase in the total conductivity was observed for La-substituted compositions, while a clear increase was achieved when the W site was replaced by Re and Mo. Substitution with 20 mol % Re led to the highest values of the total conductivity in the intermediate- to high-temperature range measured in wet Ar/H_2 (1.63×10^{-3} S·cm^{-1} at 600 °C and 1.35×10^{-2} S·cm^{-1} at 900 °C) compared to the nonsubstituted LWO and all other substituted LWOs. In dry Ar/H_2, 20 mol % Mo substitution achieved values of 1.72×10^{-3} S·cm^{-1} at 600 °C and 2.20×10^{-2} S·cm^{-1} at 900 °C and had a higher positive impact on the conductivity than 20 mol % Re substitution. The fact that these two compounds showed the highest total conductivity suggests that the higher reducibility of Re and Mo with regard to W could enhance n-type electronic conductivity, which would in turn improve the ambipolar conductivity and the final hydrogen permeation flux through LWO membranes.[48] The thermal expansion coefficients of LWO5.4 and 20 mol % Re-substituted and 20 mol % Mo-substituted LWOs were determined. Finally, the stability of Re- and Mo-substituted LWO compounds in reducing atmospheres was confirmed by means of XRD, Raman, and SEM.

For future use of substituted LWO as hydrogen separation membrane, three important facts must be considered. First, the raw material prices of Re and of Mo differ significantly. The price of Re is about 50 times higher than that of Mo. In order to find the best compound for practical applications the manufacturing costs for both substituents should be also taken into account. Second, the flux through a membrane depends not only on the ambipolar conductivity of the material but also on the thickness of the membrane. Therefore, in order to enhance the H_2 flux, attention must also be concentrated on manufacturing thin-layered membrane on a porous support. Finally, stability and effectiveness under realistic operating conditions should be addressed.

ASSOCIATED CONTENT

Supporting Information

SEM images of polished cross section of LWO5.4 (a), LWO-Ce1 (b), LWO-Nd1 (c), LWO-Mo20 (d), and LWO-Re20 (e) sintered at 1500 °C for 12 h with original and enhanced contrast; SEM-EDX analysis of LWO-Re20 after sintering at 1500 °C, 12 h; total conductivity of Re- or Mo-substituted LWO (1, 5, 20 mol %) in dry and wet Ar/H_2 as a function of the inverse temperature; SEM images of the surfaces of LWO-Re20 powder and LWO-Mo20 powder before and after reducing treatment in 100% H_2 at 800 °C for 12 h. This material is available free of charge via the Internet at http://pubs.acs.org.

AUTHOR INFORMATION

Corresponding Author

*E-mail: j.seeger@fz-juelich.de.

Notes

The authors declare no competing financial interest.

ACKNOWLEDGMENTS

The authors thank Dr. St. Roitsch for TEM analysis, Dr. W. Fischer and Mr. M. Ziegner for XRD analysis, and Dr. F. Tietz and Mrs. M.-T. Gerhards for thermal expansion analysis.

Financial support from the Helmholtz Association through the Helmholtz Alliance MEM-BRAIN (Initiative and Networking Fund) and the Spanish Ministry for Science and Innovation (Grants ENE2011-24761, CSD-2009-0050, and SEV-2012-0267) is gratefully acknowledged.

REFERENCES

(1) Taherparvar, H.; Kilner, J. A.; Baker, R. T.; Sahibzada, M. *Solid State Ionics* **2003**, *162−163*, 297−303.
(2) Yamaguchi, S.; Yamamoto, S.; Shishido, T.; Omori, M.; Okubo, A. *J. Power Sources* **2004**, *129*, 4−6.
(3) Maffei, N.; Pelletier, L.; Charland, J. P.; McFarlan, A. *J. Power Sources* **2005**, *140*, 264−267.
(4) Iwahara, H.; Esaka, T.; Uchida, H.; Madea, N. *Solid State Ionics* **1981**, *3−4*, 359−363.
(5) Lee, T. H.; Dorris, S. E.; Balachandran, U. *Solid State Ionics* **2005**, *176*, 1479−1484.
(6) Czyperek, M.; Zapp, P.; Bouwmeester, H. J. M.; Modigell, M.; Peinemann, K. V.; Voigt, I.; Meulenberg, W. A.; Singheiser, L.; Stöver, D. *Energy Procedia* **2009**, *1*, 303−310.
(7) Czyperek, M.; Zapp, P.; Bouwmeester, H. J. M.; Modigell, M.; Ebert, K.; Voigt, I.; Meulenberg, W. A.; Singheiser, L.; Stöver, D. *J. Membr. Sci.* **2010**, *359*, 149−159.
(8) Lin, Y. S. *Sep. Purif. Technol.* **2001**, *25*, 39−55.
(9) Hamakawa, S.; Li, L.; Li, A.; Iglesia, E. *Solid State Ionics* **2002**, *148*, 71−81.
(10) Song, S.-J.; Wachsman, E. D.; Rhodes, J.; Dorris, S. E.; Balachandran, U. *Solid State Ionics* **2004**, *167*, 99−105.
(11) Cheng, S.; Gupta, V. K.; Lin, J. Y. S. *Solid State Ionics* **2005**, *176*, 2653−2662.
(12) Matsumoto, H.; Shimura, T.; Higuchi, T.; Tanaka, H.; Katahira, K.; Otake, T.; Kudo, T.; Yashiro, K.; Kaimai, A.; Kawada, T.; Mizusaki, J. *J. Electrochem. Soc.* **2005**, *152*, A488−A492.
(13) Cai, M.; Liu, S.; Efimov, K.; Caro, J.; Feldhoff, A.; Wang, H. *J. Membr. Sci.* **2009**, *343*, 90−96.
(14) Wei, X.; Kniep, J.; Lin, Y. S. *J. Membr. Sci.* **2009**, *345*, 201−206.
(15) Zhana, S.; Zhu, X.; Ji, B.; Wang, W.; Zhang, X.; Wang, J.; Yang, W.; Lin, L. *J. Membr. Sci.* **2009**, *340*, 241−248.
(16) Escolástico, S.; Ivanova, M.; Solís, C.; Roitsch, S.; Meulenberg, W. A.; Serra, J. M. *RSC Adv.* **2012**, *2*, 4932−4943.
(17) Qi, X. W.; Lin, Y. S. *Solid State Ionics* **2000**, *130*, 149−156.
(18) Shimura, T.; Fujimoto, S.; Iwahara, H. *Solid State Ionics* **2001**, *143*, 117−123.
(19) McCarthy, G. J.; Fischer, R. D.; Johnson, G. G.; Gooden, J.; Gooden, C. E. *J. Solid State Chem.* 1972, National Bureau of Standards Special Publication *364*, 397−411.
(20) Ivanova, M. M.; Balagina, G. M.; Rode, E. Ya. *Inorg. Mater. (USSR)* **1970**, *6*, 803.
(21) Yoshimura, M.; Rouanet, A. *Mater. Res. Bull.* **1976**, *11*, 151−158.
(22) Magrasó, A.; Frontera, C.; Marrero-López, D.; Núñez, P. *Dalton Trans.* **2009**, 10273−10283.
(23) Ivanova, M. E.; Seeger, J.; Serra, J. M.; Solis, C.; Meulenberg, W. A.; Fischer, W.; Roitsch, S.; Buchkremer, H. P. *Chem. Mater. Res.* **2012**, *2*, 56−81.
(24) Scherb, T. Ph.D. thesis; Technische Universität Berlin 2011, doi: http://dx.doi.org/10.5442/d0014.
(25) Magrasó, A.; Polfus, J. M.; Frontera, C.; Canales-Vázquez, J.; Kalland, L.-E.; Hervoches, C. H.; Erdal, S.; Hancke, R.; Saiful Islam, M.; Norby, T.; Haugsrud, R. *J. Mater. Chem.* **2012**, *22*, 1762−1764.
(26) Magraso, A.; Hervoches, C. H.; Ahmed, I.; Hull, S.; Nordstrom, J.; Skilbred, A. W. B.; Haugsrud, R. *J. Mater. Chem. A* **2013**, *1*, 3774−3782.
(27) Scherb, T.; Kimber, S. A. J.; Stephan, C.; Henry, P. F.; Schumacher, G.; Just, J.;Escolastico, S.; Serra, J. M.; Seeger, J.; Hill, A. H.; Banhart, J. Submitted for publication, 2013.
(28) Haugsrud, R. *Solid State Ionics* **2007**, *178*, 555−560.
(29) Haugsrud, R.; Fjeld, H.; Haug, K. R.; Norby, T. *J. Electrochem. Soc.* **2007**, *154*, B77−B81.
(30) Haugsrud, R.; Kjølseth, C. *J. Phys. Chem. Solids* **2008**, *69*, 1758−1765.
(31) Serra, J. M.; Escolastico, S.; Ivanova, M.; Meulenberg, W. A.; Buchkremer, H.-P.; Stöver, D. German Patent DE102010027645.6, WO 2012/010386 A1, 2010.
(32) Amsif, M.; Magrasó, A.; Marrero-López, D.; Ruiz-Morales, J. C.; Canales-Vázquez, J.; Núñez, P. *Chem. Mater.* **2012**, *24*, 3868−3877.
(33) Zayas-Rey, M. J.; dos Santos-Gómez, L.; Marrero-López, D.; León-Reina, L.; Canales-Vázquez, J.; Aranda, M. A. G.; Losilla, E. R. *Chem. Mater.* **2013**, *25*, 448−456.
(34) Solís, C.; Escolástico, S.; Haugsrud, R.; Serra, J. M. *J. Phys. Chem. C* **2011**, *115*, 11124−11131.
(35) Escolástico, S.; Vert, V. B.; Serra, J. M. *Chem. Mater.* **2009**, *21*, 3079−3089.
(36) Escolástico, S.; Solís, C.; Serra, J. M. *Int. J. Hydrogen Energy* **2011**, *36*, 11946−11954.
(37) Escolástico, S.; Solís, C.; Serra, J. M. *Solid State Ionics* **2012**, *216*, 31−35.
(38) Pechini, M. P. U.S. Patent No. 3 330 697, 1967.
(39) Balaguer, M.; Solís, C.; Serra, J. M. *J. Phys. Chem.* **2012**, *C 116*, 7975−7982.
(40) Shannon, R. D. *Acta Crystallogr., Sect. A* **1976**, *32*, 751−767.
(41) Escolástico, S.; Solís, C.; Scherb, T.; Schumacher, G.; Serra, J. M. *J. Membr. Sci.* **2013**, *444*, 276−284.
(42) Yamanaka, S.; Fujikane, M.; Hamaguchi, T.; Muta, H.; Oyama, T.; Matsuda, T.; Kobayashi, S.-I.; Kurosaki, K. *J. Alloys Compd.* **2003**, *359*, 109−113.
(43) Serra, J.; Meulenberg, W. A. *J. Am. Ceram. Soc.* **2007**, *90*, 2082−2089.
(44) Tietz, F. *Ionics* **1999**, *5*, 129−139.
(45) Shiratori, Y.; Tietz, F.; Buchkremer, H. P.; Stöver, D. *Solid State Ionics* **2003**, *164*, 27−33.
(46) Hartmann, T.; Ehrenberg, H.; Miehe, G.; Wltschek, G.; Fuess, H. *J. Solid State Chem.* **1999**, *148*, 220−223.
(47) Dilawar, N.; Mehrotra, S.; Varandani, D.; Kumaraswamy, B. V.; Haldar, S. K. *Mater. Charact.* **2008**, *59*, 462−467.
(48) Escolástico, S.; Seeger, J.; Roitsch, S.; Ivanova, M.; Meulenberg, W. A.; Serra, J. M. *Chem. Sus. Chem.* **2013**, *6*, 1523−1532.